crystals

MDPI

Article

Motility Suppression and Trapping Bacteria by ZnO Nanostructures

Ningzhe Yan, Hao Luo *, Yanan Liu, Haiping Yu * and Guangyin Jing

School of Physics, Northwest University, Xi'an 710069, China; yanningzhe@foxmail.com (N.Y.); yanan.liu@nwu.edu.cn (Y.L.); jing@nwu.edu.cn (G.J.)
* Correspondence: luo@nwu.edu.cn (H.L.); yuhp@nwu.edu.cn (H.Y.)

Abstract: Regulating the swimming motility of bacteria near surfaces is essential to suppress or avoid bacterial contamination and infection in catheters and medical devices with wall surfaces. However, the motility of bacteria near walls strongly depends on the combination of the local physicochemical properties of the surfaces. To unravel how nanostructures and their local chemical microenvironment dynamically affect the bacterial motility near surfaces, here, we directly visualize the bacterial swimming and systematically analyze the motility of *Escherichia coli* swimming on ZnO nanoparticle films and nanowire arrays with further ultraviolet irradiation. The results show that the ZnO nanowire arrays reduce the swimming motility, thus significantly enhancing the trapping ability for motile bacteria. Additionally, thanks to the wide bandgap nature of a ZnO semiconductor, the ultraviolet irradiation rapidly reduces the bacteria locomotion due to the hydroxyl and singlet oxygen produced by the photodynamic effects of ZnO nanowire arrays in an aqueous solution. The findings quantitatively reveal how the combination of geometrical nanostructured surfaces and local tuning of the steric microenvironment are able to regulate the motility of swimming bacteria and suggest the efficient inhibition of bacterial translocation and infection by nanostructured coatings.

Keywords: ZnO nanowire arrays; bacteria motility; antibacterial; particle tracking

Citation: Yan, N.; Luo, H.; Liu, Y.; Yu, H.; Jing, G. Motility Suppression and Trapping Bacteria by ZnO Nanostructures. *Crystals* **2022**, *12*, 1027. https://doi.org/10.3390/cryst12081027

Academic Editor: Witold Łojkowski

Received: 31 May 2022
Accepted: 20 July 2022
Published: 23 July 2022

1. Introduction

The migration, colonization, and reproduction of bacteria play pivotal roles in human health and the ecological environment. Biofilm formation, for example, is a response to most inflammation and metabolism [1–4], and some bacteria can accelerate the decomposition of minerals and extract some metal materials [5,6]. The living activities of bacteria are almost entirely conducted within the confined walls of their habitat; thus, detailed bacterial movements near the surface have attracted extensive interest [7–9]. The complex geometry of real wall surfaces and the dynamical fluctuation of local environments within the immediate interfacial layer are nevertheless essential to bacterial motion and thus their attachment or detachment behavior. The swimming behaviors of bacteria driven by the flagella connected to the rotating motors on the cell membrane demonstrate fascinating features from the hydrodynamic point of view [10]. Berg and Turned [11] reported the clockwise (CW) circular motion parallel to a rigid surface due to the balance of angular momentum between the counter-rotations of flagella and body, which inevitably increased the trapping probability of bacteria near the surface. The dynamic tracking method has been proposed to directly observe the 3D trajectories of bacteria near solid surfaces under microscopy [12,13], showing that the swimming speed and tumble frequency on surfaces were lowered to a certain extent. It has been elucidated that a solid wall is able to attract bacteria with the mechanism of bacterial circular motion on the surface [14,15]. The near-surface movement of bacteria is determined to be a form of ultra-low flight [16] with an accumulation at a distance of 500 nm away from the surface, which has been further measured by Total Internal Reflection microscopy [17,18].

Except for the hydrodynamic origin of slowing down close to the surface, the physical contact between the flagellum and surface has been proven by directly capturing the collision and scattering processes [19]. It is well accepted that the steric interaction between bacteria and surfaces is also important to the motile behavior near the surfaces [20–25]. Since the bacteria swim the distance to the surface down to sub-hundred nanometers, the physicochemical properties of the surface play vital roles in movement behavior. Hu et al. [26], through their mesoscale hydrodynamic simulations, found that a change in surface roughness at the nanoscale was perceivable by cells. When bacteria swim distances of hundreds of nanometers, there is a critical slip length of about 30 nm, over which bacteria swim straight or even reverse the circular motion. In addition, charge density, wettability, and the stiffness of the surface have unavoidable influences on bacterial motility [27,28]. The motility, a measure of the swimming capability of the bacteria, is represented here by the average speed calculated from a vast number of tracked trajectories. However, most studies of bacterial contamination on surfaces roughly relied on the global adsorption number and reproduction rate of bacteria [29–33]. In contrast to adhesion, dynamical bacterial motility on rough substrates is still lacking [31–36]. Obviously, the motility of bacteria near the surface directly relates to bacterial spreading and colonization. Chang et al. found that when the surface structure size is smaller than a lower limit, the bacteria cannot feel the topography; when the structure size is around a critical value, the bacteria are more likely to travel parallel to the local crystal axis [36]. Quantitative and systematical analysis of the effect of surface topography on bacteria from both the trajectories and velocities of bacteria are rather rare. In addition, for real surfaces, such as real skin, nasal mucosa, and intestinal surfaces, except for the surface topography, the chemical microenvironment near the surface also affects bacterial behavior. As addressed in the review by Kołodziejczak-Radzimska et al. [37], the investigation of bacterial movement subjected to surfaces with complex textures and fluctuated chemical reactions are even more demanding. Particularly, from the point of view of the microscopic bacteriostasis mechanism, nanostructured coatings are excellent for capturing the physicochemical picture of modeling real surfaces, where surface morphology and the chemical microenvironment immediately near the surface (nanoscale) are both present in a natural way.

Here we use ZnO nanowire arrays (NWA) as a model system in vitro to demonstrate how the surface structures and local chemical microenvironment controlled by ultraviolet (UV) light are able to efficiently regulate bacterial swimming and quantitively evaluate the bacteriostasis merits. The tracking protocol and statistical analysis of a vast number of trajectories of individual bacteria are proposed to quantify the swimming behavior on a nanoparticles film (NPF) and NWA. Due to the photocatalytic effect of ZnO, the antibacterial components are generated at the interface under ultraviolet light irradiation and diffuse into the bulk liquid. A great number of detailed trajectories and the swimming speed of *E. coli* on different surfaces with nanostructures and under exposure to UV irradiation are systematically analyzed. It is realized that ZnO nanostructures are successful at suppressing bacterial motility within a quarter of an hour, and the spatial spreading of the bacteria is thus restricted. Interestingly, UV irradiation is found to enhance the slowing down of bacterial swimming on ZnO NWA. Our results help to understand the impact of real surfaces on bacterial motile behavior and provide a potential protocol and a general method to improve the sterilization efficiency for nanostructured materials.

2. Materials and Methods

2.1. Bacteria Culturing

E. coli (strain of RP437) with a plasmid fluorescence of protein marker YFP [38] (EX 489–505 nm, EM 524–546 nm) was used in all of the experiments. The bacterial cells were grown overnight in 15 mL of LB buffer (0.01 g/g NaCl (OXOID, Basingstoke, UK), 0.01 g/g of Tryptone (OXOID), and 0.005 g/g of Yeast (OXOID) and dissolved in DI (deionized water) culture medium, plus antibiotics (Chloramphenicol (Aladdin, Shanghai, China), 1 μL/mL), in the incubator at a temperature of 30 °C, under a shaking speed of 200 rpm. Then the

culture solution was diluted by DI water at a ratio of 1:100 into fresh medium (15 mL LB) and was kept for another growth period of 5.5 h until it reached the exponential growth phase (optical density ~0.7 at 600 nm of wavelength). The harvesting time was determined under the microscope when the bacteria presented with uniform body dimensions (about 2 μm in length and 0.5 μm in diameter) and the highest motility (~25 μm/s on average). Then, the bacterial cells were concentrated from the culture media by centrifugation (1500× *g*, 5 min), followed by the removal of the supernatant, and were then gently redispersed into the motility buffer (100 mM EDTA, 1 mM L-methionine (Sigma-Aldrich, St. Louis, MO, USA), 1 M of sodium lactate (Sigma-Aldrich) and 0.1 M of potassium phosphate buffer (EMSURE), pH = 7, and dissolved in DI water and 0.025 g/mL L-Serine (Sigma-Aldrich). The final bacteria concentration used in the tracking experiment on the glass slides and ZnO nanostructured surfaces was about 0.05 of the optical density, dissolved in motility buffer + L-Serine.

2.2. ZnO Nanostructures Preparation

ZnO NPF and NWA were synthesized using classical protocols [39]. Briefly, the glass substrate was first cleaned by ultrasonication in acetone, ethanol, and DI water for 15 min in sequence. Then, 1.44 g of $Zn(CH_3COO)_2 \cdot 2H_2O$ (Alfa Aesar, Haverhill, MA, USA), 0.75 g of PVA17-88 (Aladdin), and 1 mL of absolute ethyl alcohol (General-Reagent, Merck KGaA, Germany) were dissolved in 10 mL of DI water under constant stirring and heated for 30 min to prepare a seed layer solution. Then, a uniform, thin gel layer of the seed layer solution was spin-coated onto the substrate (10 s at 500 rpm followed by 20 s at 3000 rpm), which was transformed into ZnO NPF after annealing in a Muffle furnace (heating speed 5 °C/min, 450 °C in air, for 120 min). The substrate with ZnO NPF was placed upside down in a Teflon container and immersed in a so-called hydrothermal solution (3.5 mM $Zn(NO_3)_2 \cdot 6H_2O$ (Sigma-Aldrich) and 3.5 mM Hexamethylenetetramine (HMTA, Alfa Aesar) dissolved in 35 mL DI water) for 4 h of growth at 95 °C. After cooling down to room temperature, the ZnO NWAs grown from the seed layers were washed with ethanol and DI water several times. Finally, the wurtzite ZnO NWAs were post-annealed in a Muffle furnace (heating speed 5 °C/min, 450 °C in air, hold for 120 min) to remove the residues. The scanning electron microscopy images (SEM, FEI Apreo S, Thermo Fisher Scientific, Waltham, MA, USA), at 10 kV acceleration voltage and 11 mm of working distance) of the ZnO nanostructures are shown in Figure 1b–e. The nanowires were measured and had dimensions of 140 ± 14 nm in diameter, 8.1 ± 1.3 μm in length, 140 nm in spacing, and 21/μm^2 in number density. The grain size of the NPF was about 42.6 ± 6.1 nm in diameter and 576/μm^2 in number density (~50 nanowires or nanoparticles within 100 square microns have been selected for this statistical measurement). The roughness is defined here as the ratio of the actual area to the projected area. Then the roughness of NWA was about 96.6, which is much larger than 2.6 of NPF.

2.3. Observation Setup

A Nikon Eclipse Ti2 inverted microscope combined with a 60X Nikon (Tokyo, Japan) water immersion objective with a 1.20 numerical aperture was used for observation. Fluorescent and bright field image sequences were captured using a Flash 4.0 camera with a field-view size of 225 μm in a square at a resolution of 2048 × 2048 pixels and a framerate of 50 fps at an exposure time of 20 ms. Drops of bacterial suspension with a ~10 μL volume were transferred onto the substrates and enclosed in a 1.0 × 1.0 cm^2 chamber (Gene Frame, Thermo AB-0576, with a height of 250 μm (Figure 1a). The temperature was fixed at 24 ± 2 °C for all of the experiments. The peak wavelength of the UV light used here was about 398 nm, and the wavelength range at half maximum was 390-406 nm. The energy density of the UV light irradiated on the sample was about 4 mW/cm^2.

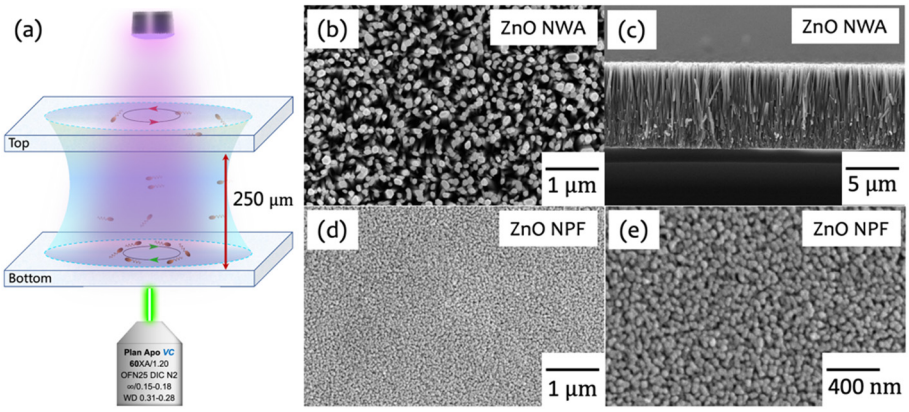

Figure 1. Experimental setup and SEM images of ZnO nanostructures. (**a**) Schematic bacterial swimming within the sandwich confinement. The bacterial suspension is surrounded by four plastic side walls to avoid evaporation. (**b**,**c**) are SEM images of ZnO NWA from the top and side view, respectively. (**d**,**e**) are SEM and zoom-in images of ZnO NPF from the top view at different magnifications, respectively.

2.4. Bacteria Tracking

The swimming bacteria on the surface were recorded by the camera as an image sequence, and the swimming path was then extracted from the linking positions of the tracked individual bacteria at a continuous time sequence. The tracking plugin of TrackMate (Fiji, NIH) was used to detect and analyze the real paths of the swimming bacteria. The displacement and speed were then calculated and plotted with MATLAB coding. Note that the bacteria suspension was rather dilute and that the interaction between each other can be neglected. Meanwhile, roughly tens to hundreds of the total number of independent trajectories were needed for our statistical analysis. To avoid damage or the photobleaching effect of the fluorescence illumination by the laser light source, each image stack was independently captured at different locations (at least 400 μm at the distance with 30% of the total fluorescence intensity).

3. Results and Discussion

3.1. Swimming on ZnO NWA

From the SEM measurements, the ZnO nanowires have a typical diameter of ~140 nm and a height of ~8.1 μm. The body (head) of the *E. coli* has a rod shape, which is about 2 μm in length and 0.5 μm in radius and is connected to 4–6 left-handed flagellum. Each flagellum is about 20 nm in diameter, 200 nm in helical radius, and 5~7 μm in length [40]. Due to the large body size of the bacteria, they are unable to penetrate into gaps between the nanoarrays. However, the rotating flagella are able to sense the ZnO NWA due to its very small diameter and large length. Therefore, the swimming behavior is expected to be different from that on ideal smooth surfaces. The swimming of bacteria on the ZnO NWA was traced with time intervals of 2 min. The typical evolving trajectories of bacterial swimming near the surface are displayed in Figure 2a, with a view field of 225×225 μm^2. As shown in Figure 2b, all of the trajectories are overlapped together with the same start point at the origin of the coordinates. In the first minute, the average moving range of swimming bacteria is about 100 μm, and some of the bacteria could reach 200 μm. While only a few bacteria could move more than 100 μm after 5 min (the majority of the motion range is less than 50 μm). Obviously, the length of the trajectory monotonically decreases over time, as shown in Figure 2a, b, indicating that the spreading of bacteria is significantly inhibited.

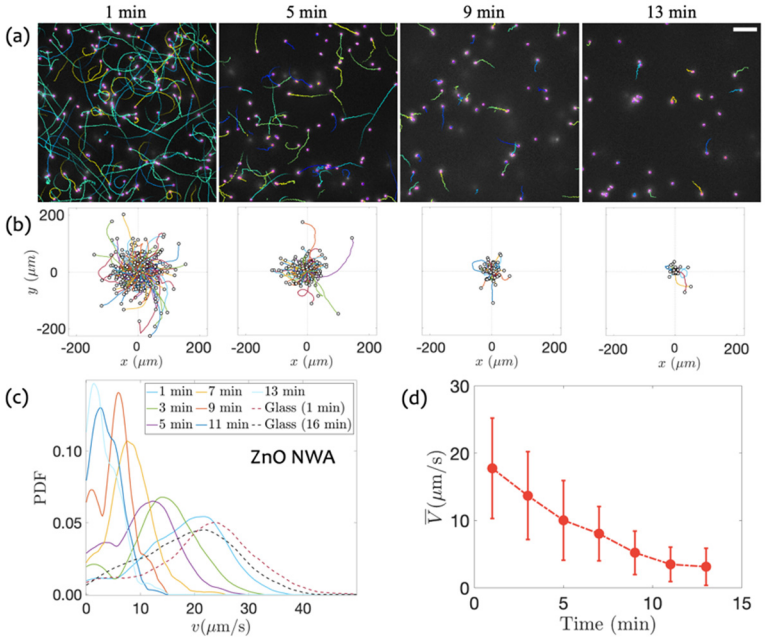

Figure 2. Swimming trajectories and motility variation on ZnO NWA. (**a**) Bacteria trajectory varying with time from 1 min to 13 min. Each trajectory is observed with a duration longer than 2 s at the focal plane. (**b**) All the trajectories are overlapped into a centered start point. (**c**,**d**) Probability density function and mean swimming speed, respectively. The scale bar represents 30 µm.

To quantify the motility of the bacteria, the instantaneous swimming speed at each time step (0.02 s) and probability density function (PDF) during each observation time window are calculated and plotted in Figure 2c. Immediately after being transferred onto the NWA from the motility buffer, the bacteria motions show that the standard variation of the swimming speed is rather wide in the beginning and then significantly shrinks with time. Moreover, the peaks of PDF gradually shift leftwards, i.e., the smaller speed region, indicating the decay of swimming motility. Furthermore, to confirm the motility supersession resulting from the ZnO NWA, the control experiment of bacteria swimming on bared glass is conducted. A glass substrate with a roughness of about 1 nm in magnitude of order measured by atomic force microscopy is a good control with a completely different material nature to ZnO nanostructured substrates. The results are shown in Figure 2c, with the red and black dashed line, respectively, which illustrate the weak decay of bacteria motility. It can also be seen that the swimming speed on the glass surface is almost maintained during the total observation time, which clearly testifies the reduction in motility due to the presence of ZnO NWA. The mean speed with error bar (standard deviation SD $= \sqrt{\frac{\Sigma\left|V-\overline{V}\right|^2}{N}}$) over time is also calculated and showed in Figure 2d, presenting the speed dropping from 17.7 µm/s to 3.1 µm/s within 12 min. Therefore, the interactions between the nanoarrays and the swimming bacteria are expected to contribute to the drag forces and the slowing down of bacterial swimming. However, as a complex interface (not ideal flat and chemical homogeneity), ZnO NWA plays a complicated role in the motility reduction in the swimming bacteria when considering the possible steric force, van der Waals force, hydrodynamic attraction with the virtual image swimmer in theoretical modeling, and the dynamical bouncing force due to the direct mechanical contact between flagella and the nanowires.

3.2. Swimming on ZnO NWA in Response to UV Irradiation

Thanks to ZnO being a wide bandgap semiconductor, UV illumination contributes to the generation of electron–hole pairs. The excess electrons are able to activate possible photodynamic effects or increase the charge density on the surfaces of the ZnO NWA.

Therefore, motility suppression and then effective attachment are expected. Then, the bacterial motility on the ZnO NWA under UV irradiation is measured. During the observation of bacterial swimming, the UV light is kept running at all times. At the initial stage, shown in Figure 3a, the bacteria swim with curved trajectories, showing the run-and-tumble process similar to that in the absence of UV light. Thereafter, the extent of the sticking and motility reduction are increasingly enhanced. Within the first minute, the length of the trajectories is almost around 50 µm, much shorter than the displacements in the absence of UV light. After 12 min, almost all of the bacteria stick to the surface and could not escape from the surface again during the observation time. Overall, the expansion range of bacterial motion became significantly smaller than that without UV irradiation, as illustrated in Figure 3c, d with the speed distribution and the mean value. It is possible that bacteria become non-motile after introducing the UV irradiation since the fluorescence of the mutation *E. coli* disappeared.

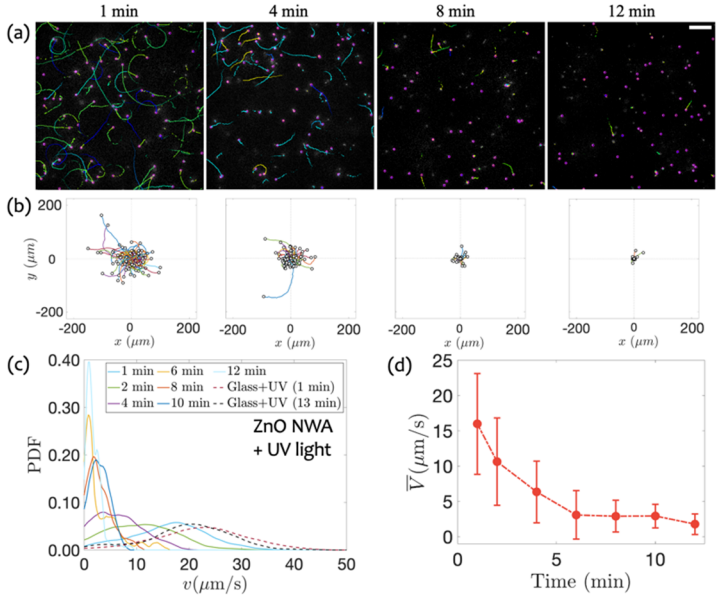

Figure 3. Bacterial swimming under UV irradiation on ZnO NWA. (**a**,**b**) Typical trajectories of swimming bacteria on NWA with varying time. (**c**,**d**) Speed distribution and mean speed at different time duration, respectively. A control experiment of bacteria swimming on bared glass under UV light is also plotted in (**c**). Scale bar is 30 µm.

To evaluate the effect of UV illumination on the swimming speed, a control experiment is carried out with UV light on bare glass under the same conditions. Figure 3c shows all the probability density distributions of the swimming speed on both the surfaces of glass and ZnO NWA under UV irradiation. It is confirmed that the UV light played a negligible role for those bacteria swimming on the glass surface without ZnO mediation, which will also be discussed in a later section.

3.3. Swimming on ZnO NPF with and without UV Radiation

To identify the influence of surface morphology on bacterial motility, a nanoparticle film of ZnO is used as a counterpart to the nanowire array. From the SEM measurements (Figure 1d, e), the NPF consisted of nanosized particles with a diameter of ~42.6 nm. Figure 4a shows the typical bacterial trajectories over time on the NPF without UV irradiation. As shown in Figure 4d, the movement range of bacteria during the tracked period can reach 200 µm in 1 min, with a typical value of 150 µm. At 9 min, only a few bacteria can spread around 100 µm. A long time later (37 min), the range of bacterial motion shrinks slightly. The mean swimming speed shown in Figure 4g, reaches a plateau in 13 min, and the mean speed drops to 5.6 µm/s in 37 min from the initial speed of 17.7 µm/s.

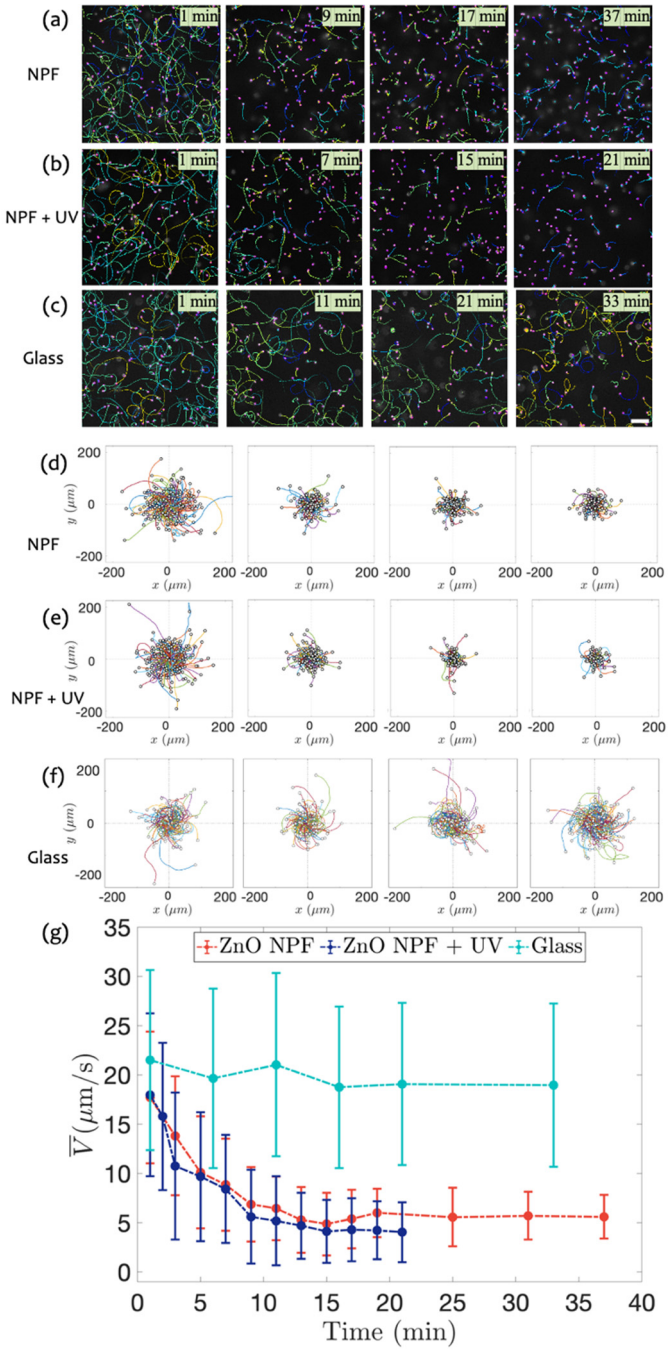

Figure 4. Swimming on nanoparticle film of ZnO. (**a**–**f**) Snapshots and trajectories of tracked bacteria on NPF and glass with and without UV irradiation, respectively. (**g**) Mean swimming speed on NPF with and without UV irradiation over time. The scale bar represents 30 μm.

Then, the bacteria motility on the ZnO NPF with UV irradiation is also measured and shown in Figure 4b,e. After 1 min, the motion range of bacteria during the tracking period can reach 200 μm, very close to that of those swimming on glass and ZnO NWA with and without UV light. Compared with the data of ZnO NWA under UV irradiation, the shift and contraction of peak positions are not sharp. The mean bacteria motility over time with an error bar, calculated by the standard deviation of each trajectory, is shown in Figure 4g, where a negligible decrease occurs, and the mean speed drops from 18.0 to 4.0 μm/s in 21 min. Most of the bacteria on ZnO NPF + UV lose their fluorescence after 21 min, resulting in the number of bacteria not reaching the minimum.

3.4. Comparison of Bacterial Motility

The anti-contamination efficiency of physical structures and chemical reactions due to the coupling of photon–electron and UV illumination is now evaluated. The experiments about the effect of UV irradiation are carried out on three types of substrates, including bared glass, ZnO NPF, and ZnO NWA. As shown in Figure 5a, there are basically no differences in the speed of the bacteria in the two groups of experiments on glass with and without UV illumination marked with the colors cyan and purple, respectively, indicating the negligible effect of the UV light for swimming bacteria on a glass surface. Here, the error bar and data after 15 min are hidden in Figure 5a for clearer alignment. The mean speed on the ZnO NPF shows a substantial reduction, implying a specific contribution from the material nature of ZnO. Furthermore, the motility of bacteria on the ZnO NWA is also slightly lower than that on the ZnO NPF, suggesting that the physical barriers created by roughness have a weak effect on bacterial motility. However, a distinct decay of mean speed appears on ZnO NWA with UV irradiation, i.e., the mean speed dropped to 3.5 μm/s after 6 min, which is faster than that without UV irradiation. The apparent enhancement of bacteriostatic ability illustrates that the roughness of the nanowire arrays plays a weak role from nanoparticle to nanoarray while significantly contributing to motility suppression due to chemical reactions by converting photonic energy to excess electrons.

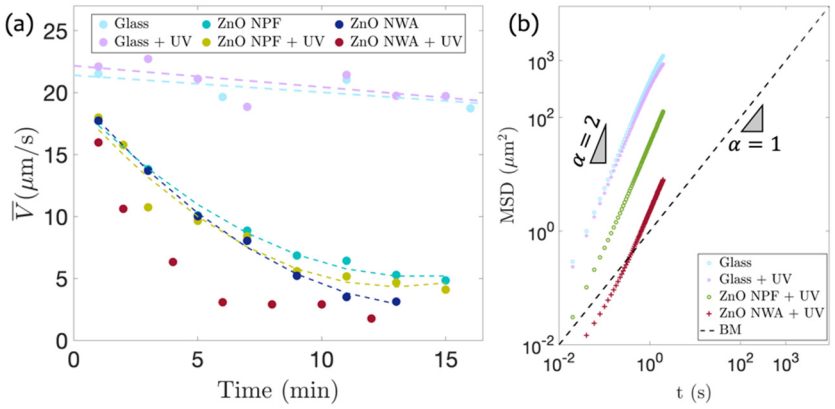

Figure 5. Mean speed and ballistic diffusion of bacterial spreading on various surfaces with and without UV irradiation. (**a**) Replot of bacterial motility as a function of time on ZnO NWA, ZnO NPF, and bared glass substrates, respectively. (**b**) Mean squared displacement depends on the lag time, showing the ballistic and super diffusion processes.

MSD (mean square displacement) $\langle |x(t) - x_0|^2 + |y(t) - y_0|^2 \rangle$ is used here to evaluate the spreading efficiency of bacteria on the surface based on the trajectories by the calculation of the time-evolving position $x(t)$ and $y(t)$. MSD is also ascribed to the motility of bacteria. As shown in Figure 5b, the MSD depending on lag time demonstrates a ballistic diffusion feature, i.e., MSD ~ t^2, which is reasonable by recognizing the bacteria as a type of self-propelled particles. As a reference to the Brownian motion of passive particles due to thermal agitation, polystyrene beads with a 1 μm diameter (comparable with the bacterial size) and with a density of 1.04 g/cm^3, which is also similar to that of the bacteria (1.04 g/cm^3), are used to present the spreading capability, as marked with a black dashed line in Figure 5b. In the case of ZnO NWA under UV irradiation, bacterial motility, characterized by an active ballistic diffusion process, is even smaller than that of pure Brownian particles at a short time range (less than 1 s). In other cases, bacteria behave with greater motility than Brownian particles do in the all-time window. The slopes of the four MSD curves are both greater than 1, indicating a super diffusion mode of bacterial swimming [41]. In other words, swimming bacteria, similar to typical, active Brownian particles, prefer straight motion compared to a random walk with a long-time limit.

Briefly, the motility of bacteria on ZnO was significantly inhibited compared to that on glass. This inhibition effect occurs immediately (within 1 min) after the transfer of bacteria onto ZnO nanostructures. The reduction in bacterial speed is supposed to be the reason that the ZnO nanomaterial is a typical polar material [42,43], and the oxygen vacancies on the surface can form a large number of equivalent positive charge centers [44–46], which is more likely to adsorb negatively charged *E. coli* [47]. In the absence of UV irradiation, the motility of bacteria on the ZnO NWA is slightly lower than that on ZnO NPF. It might be caused by the large undulation of the arrays, collisions, or flagella entanglement when *E. coli* swims close to the surface with a geometrical landscape. This is consistent with the more random swimming directions indicated by the trajectories of bacteria on the ZnO NWA, as shown in Figure 2.

The ZnO NWA presents a significant antibacterial effect under UV irradiation, and the corresponding enhancement effect is clear compared with results from measurements on the NPF. It is believed that the photodynamic-effect efficiency of the nanowire arrays with a large surface area comes to play an important role. The roughness is defined here as the ratio of the actual area to the projected area. Then the roughness of NWA is about 96.6, which is much larger than 2.6 of NPF. UV irradiation is adopted to generate hydroxyl radicals and singlet oxygen in the aqueous phase in the presence of ZnO, which has been proven to be curtailed [48–51], shown in the sketch of Figure 6. Compared with the insensitivity of the ZnO NPF to UV light, the higher roughness of the ZnO NWA leads to a significant improvement in the bacteriostatic effect.

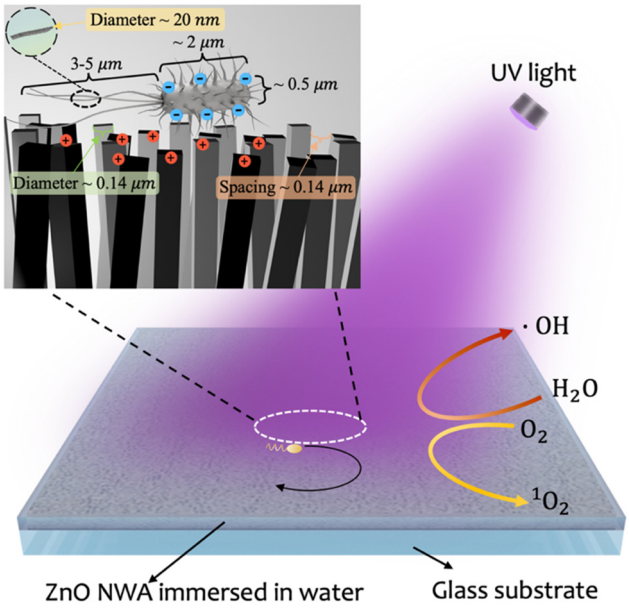

Figure 6. Sketch of bacterial swimming on ZnO NWA. Generation of hydroxyl radical and singlet oxygen are initiated in the presence of UV irradiation.

4. Conclusions

In summary, ZnO nanostructures are used to investigate the interfacial swimming behavior of *E. coli* by tuning surface textures and chemical reactions by remote undulation towards bacteriostatic capability. By visualizing the swimming trajectories of bacteria and analyzing their locomotion ability, the natural bacteriostatic ability of ZnO is quantitatively determined, showing that the average speed of bacteria can be reduced by 20% immediately after introducing ZnO nanostructures into the bacterial suspension. Increasing the roughness and the exposure of UV irradiation can further improve the antibacterial effect of the ZnO nanomaterials. Interestingly, when large roughness and UV irradiation are combined, the bacteriostatic effect is significantly enhanced. ZnO NWA with UV light irradiation reduces almost 90% of bacterial motility (slowing down to ~2 μm/s) within

only 6 min. This highly effective bacteriostatic ability might originate from the combined effect of the polar nature of ZnO crystallization, the structural properties of the nanowire arrays, and the photodynamic effects. The strong trapping ability of ZnO NWA can strongly inhibit the migration of bacteria and prevent bacterial infection. Trapped bacteria become non-motile with possible bacteriostatic substances produced by photodynamic effects from ZnO material nature. The findings here not only demonstrate the detailed motility of bacteria swimming on nanostructured surfaces but also provide means for antibacterial applications of ZnO nanomaterials.

Author Contributions: Conceptualization, N.Y., H.L. and G.J.; Methodology, N.Y., H.L. and G.J.; Software, N.Y. and Y.L.; Investigation, N.Y., H.L. and G.J.; Formal analysis, N.Y., H.L., H.Y. and G.J.; Resources, N.Y.; Data Curation, N.Y.; Writing—Review and Editing, N.Y., H.L., Y.L. and G.J.; Supervision, N.Y., H.L. and G.J.; Project administration, N.Y., H.L., H.Y. and G.J.; Funding acquisition, G.J., Y.L., H.Y. and H.L. All authors have read and agreed to the published version of the manuscript.

Funding: This research received the funding from NSFC (12004308, 12174306, 11804275), and the special Scientific Research Program of Shaanxi Provincial Education Department (No. 203010036).

Institutional Review Board Statement: Not applicable.

Informed Consent Statement: Not applicable.

Data Availability Statement: Not applicable.

Acknowledgments: The authors thanks E. Clément for providing *E. coli* RP437 bacteria, and gratefully acknowledge the help from F. Teng.

Conflicts of Interest: The authors declare no conflict of interest.

References

1. Knights, H.E.; Jorrin, B.; Haskett, T.L.; Poole, P.S. Deciphering bacterial mechanisms of root colonization. *Environ. Microbiol. Rep.* **2021**, *13*, 428–444. [CrossRef] [PubMed]
2. Gensollen, T.; Iyer, S.S.; Kasper, D.L.; Blumberg, R.S. How colonization by microbiota in early life shapes the immune system. *Science* **2016**, *352*, 539–544. [CrossRef]
3. Siegel, S.J.; Weiser, J.N. Mechanisms of bacterial colonization of the respiratory tract. *Annu. Rev. Microbiol.* **2015**, *69*, 425–444. [CrossRef] [PubMed]
4. Ribet, D.; Cossart, P. How bacterial pathogens colonize their hosts and invade deeper tissues. *Microbes Infect.* **2015**, *17*, 173–183. [CrossRef] [PubMed]
5. Bosecker, K. Bioleaching: Metal solubilization by microorganisms. *FEMS Microbiol. Rev.* **1997**, *20*, 591–604. [CrossRef]
6. Kolencik, M.; Vojtkova, H.; Urik, M.; Caplovicova, M.; Pistora, J.; Cada, M.; Babicova, A.; Feng, H.; Qian, Y.; Ramakanth, I. Heterotrophic bacterial leaching of zinc and arsenic from artificial adamite. *Water Air Soil Pollut.* **2017**, *228*, 1–11. [CrossRef]
7. Vaccari, L.; Molaei, M.; Niepa, T.H.; Lee, D.; Leheny, R.L.; Stebe, K.J. Films of bacteria at interfaces. *Adv. Colloid Interface Sci.* **2017**, *247*, 561–572. [CrossRef]
8. Alapan, Y.; Yasa, O.; Yigit, B.; Yasa, I.C.; Erkoc, P.; Sitti, M. Microrobotics and microorganisms: Biohybrid autonomous cellular robots. *Annu. Rev. Control Robot. Auton. Syst.* **2019**, *2*, 205–230. [CrossRef]
9. Raina, J.-B.; Fernandez, V.; Lambert, B.; Stocker, R.; Seymour, J.R. The role of microbial motility and chemotaxis in symbiosis. *Nat. Rev. Microbiol.* **2019**, *17*, 284–294. [CrossRef]
10. Lauga, E. Bacterial hydrodynamics. *Annu. Rev. Fluid Mech.* **2016**, *48*, 105–130. [CrossRef]
11. Berg, H.C.; Turner, L. Chemotaxis of bacteria in glass capillary arrays. Escherichia coli, motility, microchannel plate, and light scattering. *Biophys. J.* **1990**, *58*, 919–930. [CrossRef]
12. Frymier, P.D.; Ford, R.M.; Berg, H.C.; Cummings, P.T. Three-dimensional tracking of motile bacteria near a solid planar surface. *Proc. Natl. Acad. Sci. USA* **1995**, *92*, 6195–6199. [CrossRef] [PubMed]
13. Frymier, P.D.; Ford, R.M. Analysis of bacterial swimming speed approaching a solid–liquid interface. *AIChE J.* **1997**, *43*, 1341–1347. [CrossRef]
14. Lauga, E.; DiLuzio, W.R.; Whitesides, G.M.; Stone, H.A. Swimming in circles: Motion of bacteria near solid boundaries. *Biophys. J.* **2006**, *90*, 400–412. [CrossRef]
15. Lopez, D.; Lauga, E. Dynamics of swimming bacteria at complex interfaces. *Phys. Fluids* **2014**, *26*, 400–412. [CrossRef]
16. Li, G.; Bensson, J.; Nisimova, L.; Munger, D.; Mahautmr, P.; Tang, J.X.; Maxey, M.R.; Brun, Y.V. Accumulation of swimming bacteria near a solid surface. *Phys. Rev. E* **2011**, *84*, 041932. [CrossRef]

17. Vigeant, M.A.-S.; Ford, R.M.; Wagner, M.; Tamm, L.K. Reversible and irreversible adhesion of motile Escherichia coli cells analyzed by total internal reflection aqueous fluorescence microscopy. *Appl. Environ. Microbiol.* **2002**, *68*, 2794–2801. [CrossRef] [PubMed]
18. Li, G.; Tam, L.-K.; Tang, J.X. Amplified effect of Brownian motion in bacterial near-surface swimming. *Proc. Natl. Acad. Sci. USA* **2008**, *105*, 18355–18359. [CrossRef]
19. Kantsler, V.; Dunkel, J.; Polin, M.; Goldstein, R.E. Ciliary contact interactions dominate surface scattering of swimming eukaryotes. *Proc. Natl. Acad. Sci. USA* **2013**, *110*, 1187–1192. [CrossRef]
20. Vigeant, M.; Ford, R.M. Interactions between motile Escherichia coli and glass in media with various ionic strengths, as observed with a three-dimensional-tracking microscope. *Appl. Environ. Microbiol.* **1997**, *63*, 3474–3479. [CrossRef]
21. Bos, R.; Van der Mei, H.C.; Busscher, H.J. Physico-chemistry of initial microbial adhesive interactions–its mechanisms and methods for study. *FEMS Microbiol. Rev.* **1999**, *23*, 179–230. [CrossRef]
22. Hermansson, M. The DLVO theory in microbial adhesion. *Colloids Surf. B Biointerfaces* **1999**, *14*, 105–119. [CrossRef]
23. Zhao, W.; Walker, S.L.; Huang, Q.; Cai, P. Adhesion of bacterial pathogens to soil colloidal particles: Influences of cell type, natural organic matter, and solution chemistry. *Water Res.* **2014**, *53*, 35–46. [CrossRef] [PubMed]
24. Bianchi, S.; Saglimbeni, F.; Frangipane, G.; Dell'Arciprete, D.; Di Leonardo, R. 3D dynamics of bacteria wall entrapment at a water–air interface. *Soft Matter* **2019**, *15*, 3397–3406. [CrossRef]
25. Kim, D.; Kim, Y.; Lim, S. Effects of swimming environment on bacterial motility. *Phys. Fluids* **2022**, *34*, 031907. [CrossRef]
26. Hu, J.; Wysocki, A.; Winkler, R.G.; Gompper, G. Physical sensing of surface properties by microswimmers–directing bacterial motion via wall slip. *Sci. Rep.* **2015**, *5*, 1–7. [CrossRef]
27. Gottenbos, B.; Grijpma, D.W.; van der Mei, H.C.; Feijen, J.; Busscher, H.J. Antimicrobial effects of positively charged surfaces on adhering Gram-positive and Gram-negative bacteria. *J. Antimicrob. Chemother.* **2001**, *48*, 7–13. [CrossRef]
28. Zheng, S.; Bawazir, M.; Dhall, A.; Kim, H.-E.; He, L.; Heo, J.; Hwang, G. Implication of surface properties, bacterial motility, and hydrodynamic conditions on bacterial surface sensing and their initial adhesion. *Front. Bioeng. Biotechnol.* **2021**, *9*, 82. [CrossRef]
29. Schwibbert, K.; Menzel, F.; Epperlein, N.; Bonse, J.; Krüger, J. Bacterial adhesion on femtosecond laser-modified polyethylene. *Materials* **2019**, *12*, 3107. [CrossRef]
30. Chien, H.-W.; Chen, X.-Y.; Tsai, W.-P.; Lee, M. Inhibition of biofilm formation by rough shark skin-patterned surfaces. *Colloids Surf. B Biointerfaces* **2020**, *186*, 110738. [CrossRef]
31. Tang, M.; Chen, C.; Zhu, J.; Allcock, H.R.; Siedlecki, C.A.; Xu, L.-C. Inhibition of bacterial adhesion and biofilm formation by a textured fluorinated alkoxyphosphazene surface. *Bioact. Mater.* **2021**, *6*, 447–459. [CrossRef] [PubMed]
32. Du, C.; Wang, C.; Zhang, T.; Yi, X.; Liang, J.; Wang, H. Reduced bacterial adhesion on zirconium-based bulk metallic glasses by femtosecond laser nanostructuring. *Proc. Inst. Mech. Eng. Part H J. Eng. Med.* **2020**, *234*, 387–397. [CrossRef] [PubMed]
33. Lutey, A.H.; Gemini, L.; Romoli, L.; Lazzini, G.; Fuso, F.; Faucon, M.; Kling, R. Towards laser-textured antibacterial surfaces. *Sci. Rep.* **2018**, *8*, 1–10. [CrossRef] [PubMed]
34. Yang, M.; Ding, Y.; Ge, X.; Leng, Y. Control of bacterial adhesion and growth on honeycomb-like patterned surfaces. *Colloids Surf. B Biointerfaces* **2015**, *135*, 549–555. [CrossRef] [PubMed]
35. Helbig, R.; Günther, D.; Friedrichs, J.; Rößler, F.; Lasagni, A.; Werner, C. The impact of structure dimensions on initial bacterial adhesion. *Biomater. Sci.* **2016**, *4*, 1074–1078. [CrossRef]
36. Chang, Y.-R.; Weeks, E.R.; Ducker, W.A. Surface topography hinders bacterial surface motility. *ACS Appl. Mater. Interfaces* **2018**, *10*, 9225–9234. [CrossRef]
37. Kolodziejczak-Radzimska, A.; Jesionowski, T. Zinc oxide—from synthesis to application: A review. *Materials* **2014**, *7*, 2833–2881. [CrossRef]
38. Hecht, A.; Endy, D.; Salit, M.; Munson, M.S. When wavelengths collide: Bias in cell abundance measurements due to expressed fluorescent proteins. *ACS Synth. Biol.* **2016**, *5*, 1024–1027. [CrossRef]
39. Yin, Z.; Shan, Y.; Yu, M.; Yang, L.; Song, J.; Hu, P.; Teng, F. Enhanced performance of UV photodetector based on ZnO nanorod arrays via TiO2 as electrons trap layer. *Mater. Sci. Semicond. Processing* **2022**, *148*, 106813. [CrossRef]
40. Son, K.; Brumley, D.R.; Stocker, R. Live from under the lens: Exploring microbial motility with dynamic imaging and microfluidics. *Nat. Rev. Microbiol.* **2015**, *13*, 761–775. [CrossRef]
41. Wu, X.-L.; Libchaber, A. Particle diffusion in a quasi-two-dimensional bacterial bath. *Phys. Rev. Lett.* **2000**, *84*, 3017. [CrossRef] [PubMed]
42. Heiland, G.; Kunstmann, P. Polar surfaces of zinc oxide crystals. *Surf. Sci.* **1969**, *13*, 72–84. [CrossRef]
43. Ching, K.-L.; Li, G.; Ho, Y.-L.; Kwok, H.-S. The role of polarity and surface energy in the growth mechanism of ZnO from nanorods to nanotubes. *CrystEngComm* **2016**, *18*, 779–786. [CrossRef]
44. Luo, H.; Ma, J.; Wang, P.; Bai, J.; Jing, G. Two-step wetting transition on ZnO nanorod arrays. *Appl. Surf. Sci.* **2015**, *347*, 868–874. [CrossRef]
45. Pacchioni, G. Oxygen vacancy: The invisible agent on oxide surfaces. *ChemPhysChem* **2003**, *4*, 1041–1047. [CrossRef]
46. Scorza, E.; Birkenheuer, U.; Pisani, C. The oxygen vacancy at the surface and in bulk MgO: An embedded-cluster study. *J. Chem. Phys.* **1997**, *107*, 9645–9658. [CrossRef]
47. Güler, S.; Oruç, Ç. Comparison of the behavior of negative electrically charged E. coli and E. faecalis bacteria under electric field effect. *Colloids Surf. B Biointerfaces* **2021**, *208*, 112097. [CrossRef]

48. Yi, C.; Yu, Z.; Ren, Q.; Liu, X.; Wang, Y.; Sun, X.; Yin, S.; Pan, J.; Huang, X. Nanoscale ZnO-based photosensitizers for photodynamic therapy. *Photodiagnosis Photodyn. Ther.* **2020**, *30*, 101694. [CrossRef]
49. Jyothi, M.; Nayak, V.; Padaki, M.; Balakrishna, R.G.; Ismail, A. The effect of UV irradiation on PSf/TiO2 mixed matrix membrane for chromium rejection. *Desalination* **2014**, *354*, 189–199. [CrossRef]
50. Bono, N.; Ponti, F.; Punta, C.; Candiani, G. Effect of UV irradiation and TiO2-photocatalysis on airborne bacteria and viruses: An overview. *Materials* **2021**, *14*, 1075. [CrossRef]
51. Fakhar-e-Alam, M.; Kishwar, S.; Willander, M. Photodynamic effects of zinc oxide nanowires in skin cancer and fibroblast. *Lasers Med. Sci.* **2014**, *29*, 1189–1194. [CrossRef] [PubMed]